www.sciencemag.org/cgi/content/full/science.1234787/DC1

Supplementary Materials for

3D Reconstruction of the Source and Scale of Buried Young Flood Channels on Mars

Gareth. A. Morgan,* Bruce. A. Campbell, Lynn. M. Carter, Jeffrey. J. Plaut, Roger. J. Phillips

*Corresponding author. E-mail: morganga@si.edu

Published 7 March 2013 on *Science* Express
DOI: 10.1126/science.1234787

This PDF file includes:

Materials and Methods
Supplementary Text
Figs. S1 to S4
Table S1
Reference (*25*)

Materials and Methods

SHARAD

The SHARAD radar operates at a 20 MHz center frequency (15m wavelength) with a 10 MHz bandwidth, and has a free-space vertical resolution of 15 m, equivalent to a 5 – 10 m vertical resolution in common silicic geologic materials (*10*). At this wavelength SHARAD can probe up to a few hundred meters into the subsurface. With synthetic aperture focusing and depending on surface roughness, SHARAD has a spatial resolution of 300-500 m along-track and several kilometers across-track (*10, 11*). Such spatial resolution and penetration are optimal for studying Marte Vallis, which extends over hundreds of kilometers and contains volcanic and sedimentary material estimated to be less than several hundred meters thick (*5*). The young, uniform plains of Elysium Planitia are ideally suited for radar sounding, consisting of extensive near-horizontal surfaces that lack significant off-nadir clutter.

The SHARAD data for each orbital track is presented as a radargram (see Fig. 1, S1). This depicts the variations in echo strength (received from the surface and subsurface) with time delay along the MRO ground track. The y-axis of a radargram (range direction) corresponds to the round-trip delay time of the returned signal. Each pixel represents 0.0375 μs, or ~11 m round-trip vertical distance travelled in vacuum. The x-axis of a radargram plots the along-track distance traveled. Contrasts in electrical permittivity reflect the transmitted signal, and these subsurface reflections can be used to investigate geologic boundaries and stratigraphy.

The SHARAD sounding tracks used in this study were processed using a flexible synthetic aperture radar processing system. This system allows for varying synthetic aperture length and multi-look averaging, allowing a user to fine-tune the processing to maximize the signal-to-noise ratio for particular subsurface reflectors. Ionospheric distortion and delay variations of the radar signals in daytime SHARAD observations are fully compensated using an autofocus technique described by (*26*). Off-nadir reflections from surface features such as hills or ridges, termed clutter, can in some regions of Mars create complications in mapping subsurface reflecting horizons. For the generally smooth (at the km scale) Elysium Planitia, the effects of such clutter are almost negligible (e.g., *21*). Where ambiguities did arise we checked the SHARAD sounding results against simulations produced by ray tracing of MOLA gridded data, and rejected any spurious reflections.

3D Mapping

Each radargram was visually inspected and the horizontal extent of all identified subsurface reflectors was recorded (see Fig. S1, Table S1). From this the latitude and longitude coordinates and the two way time delay between each reflector and the surface was automatically extracted (using IDL) and used to create a shapefile containing all of the reflectors. ArcMap GIS software was used to explore the spatial extent of the reflectors and compare their location with other Mars datasets, including published geologic maps (Fig. S2). This process identified three separate reflector groups: L1R, L2R and R3 (Fig. 2).

Establishing the actual depth of a reflector below the surface can be estimated from the radargrams, but is dependent on knowledge of the integrated permittivity (ε′) of the material above that reflector:

$$h = \frac{\Delta t c}{2\sqrt{\varepsilon'}} \qquad (1)$$

Where Δt is the round-trip delay time between the surface and a reflector taken from the SHARAD radargram. Figure 2 displays the depth of the reflectors relative to a martian datum after assuming a subsurface value for ε′ and subtracting the converted depth from the MOLA gridded data. Based on geologic mapping of the study region (*5, 14*), which identifies the surface as volcanic in origin, we assume ε′ of 8, consistent with dense, dry terrestrial lava flows. This process removes the effects of surface elevation, making it easier to discern patterns among the different reflectors. For example, we observe that the L1R and L2R reflectors both dip toward the northeast at a similar angle as the surface (Fig. 2).

In order to investigate the spatial nature of the channels identified with the R3 reflector (Fig. 1a, S1), we interpolated across the depth estimates provided by the 21 radargrams in which occurrences of R3 were identified. This was done in ArcMap and provided a model of the subsurface horizon delimited by R3. IDL scientific data visualization software was employed to investigate the three dimensional structure of the R3 horizon and compare it spatially to other Mars datasets (Fig 3). This approach revealed that channel features all begin abruptly along an alignment that matches the orientation of Cerberus Fossae to the west (Fig. 3, S3) as established in CTX image data.

From our GIS analysis we identified spatially coherent incisions in the L1R and L2R reflectors (See Fig. S3). To generate the tomographic model of Marte Vallis, the edges of each truncation in the two reflectors (Fig 1, S1) was recorded (both spatially and in time delay) along with the surface expression of the streamlined features (identified in the MOLA gridded data) and used as control points for interpolation. The buried channels mapped through this process align with the channel features identified with the R3 reflector (Fig. S3).

Equation 1 states the depth of a reflector as constrained from a radargram is inversely proportional to ε′. As our choice of ε′ of 8 is at the high end of expected permittivities for Mars (*22, 23*), choosing a lower value would result in greater depth estimates for the Marte Vallis channels. In the manuscript we have presented a range of depth estimates for the Marte Vallis channels constrained by L1R and L2R that reflect the expected permittivity range for Mars.

Supplementary Text

Geologic History of Eastern Elysium

Summarizing our results, we can now better describe our interpretation of the sequence of geologic events that shaped eastern Elysium Planitia. Prior to flooding, the Marte Vallis region was covered in ACo volcanic terrain. Two subsurface reflectors at different depths characterize this terrain indicating broad, continuous, flat-lying units that follow the surface dip to the northeast (Fig. S4a). The origin of the materials bounded by

these reflectors is unknown, though mapping of the region suggests the upper unit is volcanic (*5, 14*). Flooding from the eastern-most section of Cerberus Fossae occurred between ~10 Ma and 500 Ma, constrained by the dating of ACo and ACy units (*5*), and eroded multiple anastomosing channels that coalesced to form Marte Vallis (Fig. S4b). Continual down cutting occurred in the southern-most channel (Fig. S4c). The final phase consisted of young volcanism and the flow of lava over ACo. The continued northeastern expansion of these flows would have flooded Marte Vallis and buried Cerberus Fossae, producing the surfaces present today (Fig. S1d).

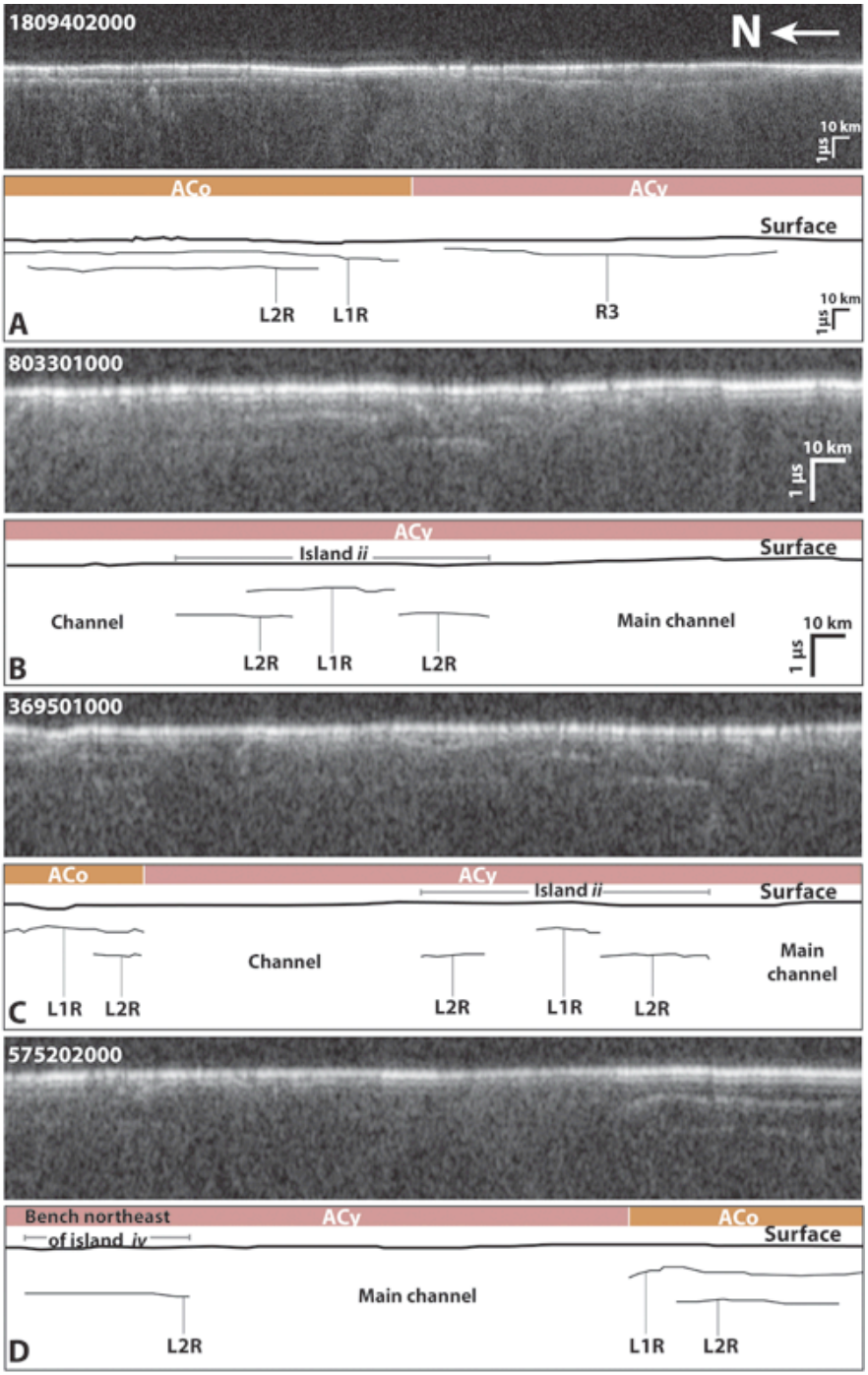

Fig. S1. Examples of radargrams and accompanying interpretations used to map Marte Vallis channels. The color bars represent geologic units from (*5*), North is to the left. Spatial coordinates of the radargram examples presented: (A) 1809402000 (9.72°N, 173.78°E – 1.02° N, 172.72° E), (B) 803301000 (8.67° N, 177.43° E – 4.32° N, 176.9° E) (C) 369501000 (9.85° N, 177.63° E – 5.5° N, 177.09° E), (D) 575202000 (8.01° N, 178.76° E – 3.66° N, 178.23° E) The locations of the SHARAD tracks are presented in Fig. S2.

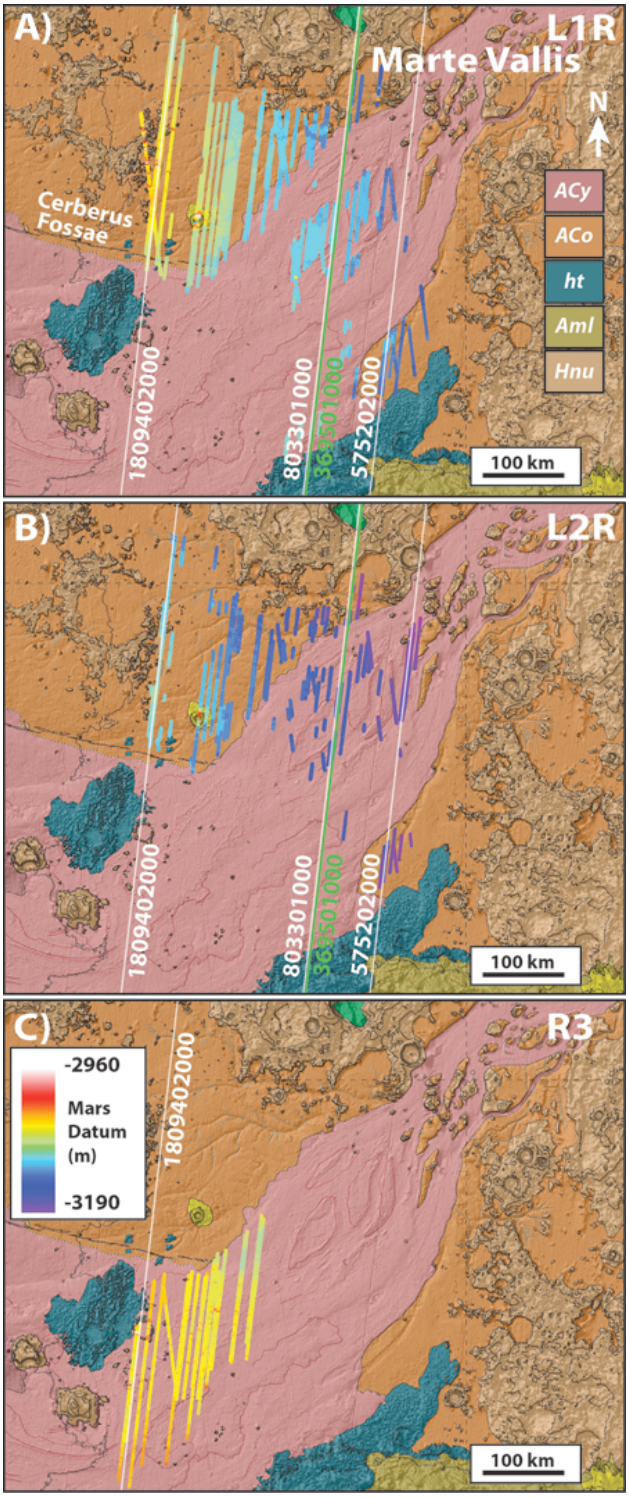

Fig. S2 Context maps of the radargrams presented in Fig. S1. Spatial distribution of L1R (A), L2R (B) and R3 (C) reflectors corrected for depth. Background shows the (*5*) geologic map overlaid on a hillshade image of MOLA gridded data (200 x vertical exaggeration). [Geologic map adapted from (*5*) with permission from Elsevier]

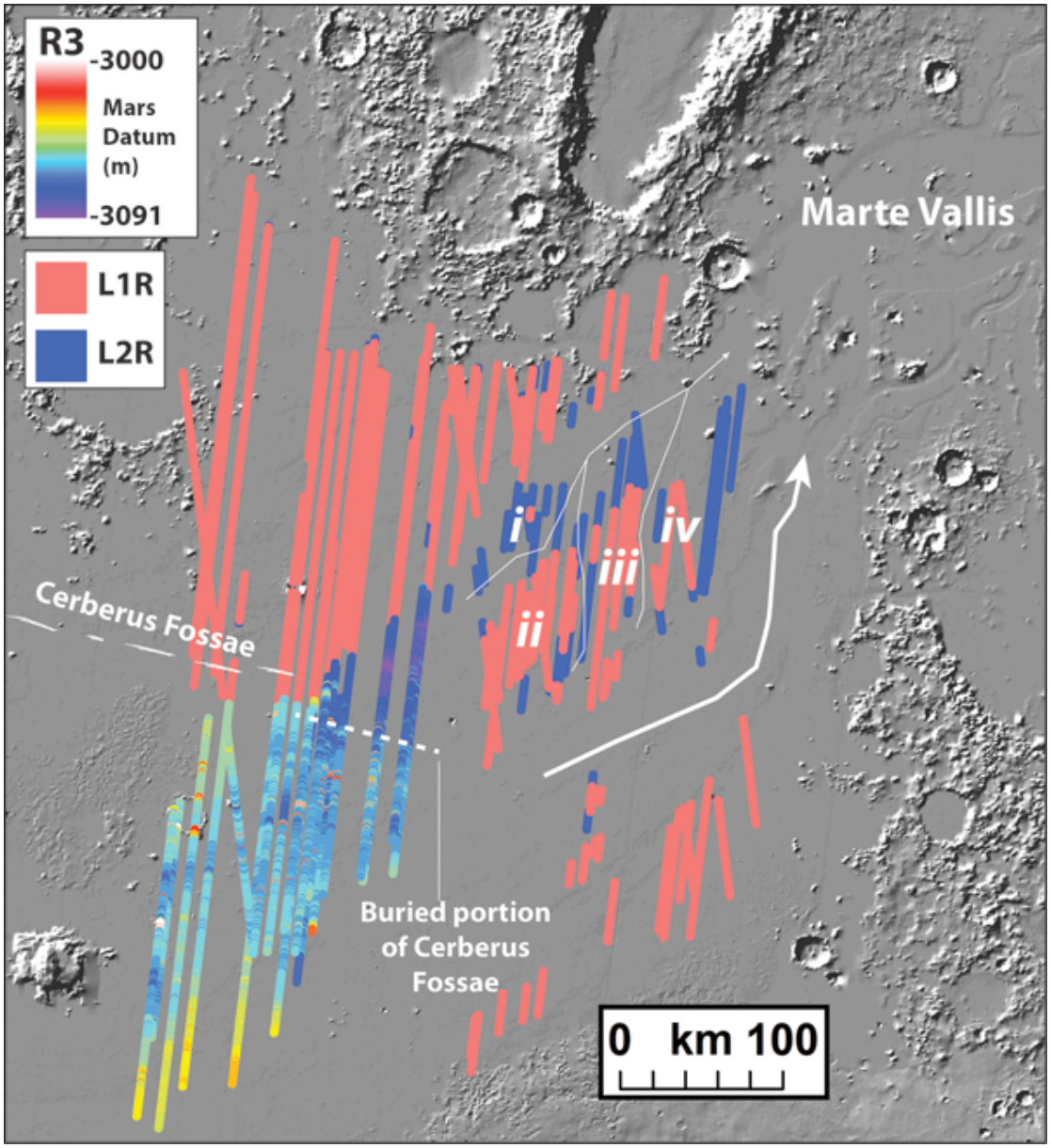

Fig. S3 Depth of R3 reflector from SHARAD data, stretched to highlight the Marte Vallis channels identified in the radargrams (See Fig 1a). Note that the channels begin abruptly along an orientation that matches Cerberus Fossae to the west. The location of L1R and L2R reflectors is also shown. White arrows indicate inferred flow direction along the truncations in the reflectors. Note that the channels identified in R3 align with the incisions in the L1R reflector. North is to the top of the figure.

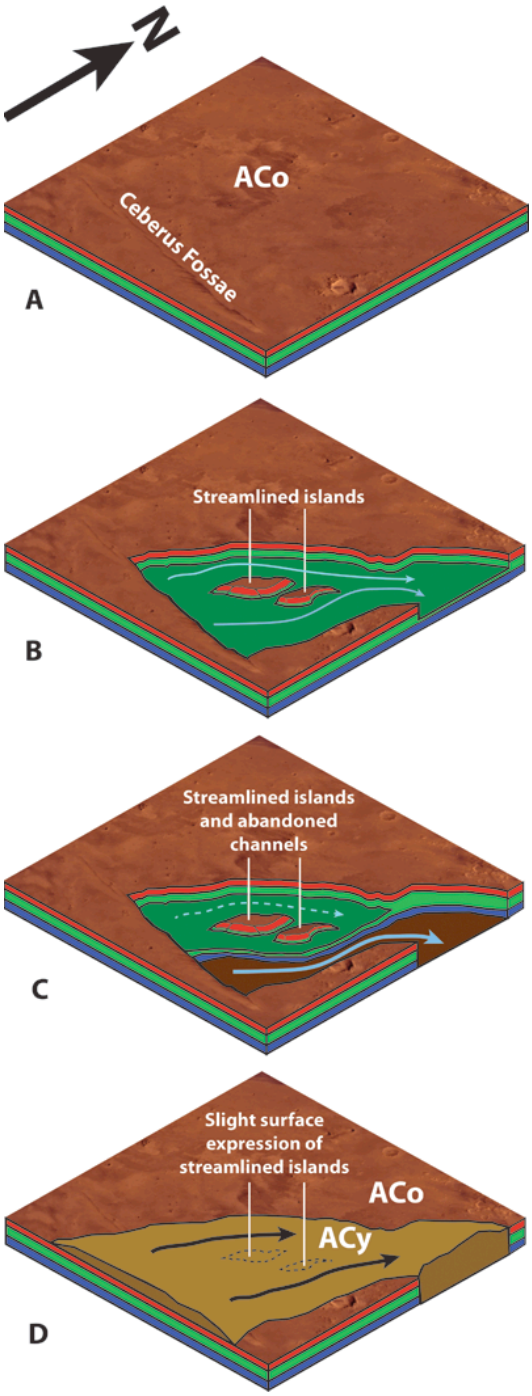

Fig. S4 Schematic history of the region as interpreted from SHARAD data. (A) Pre-flood, Unit ACo covers the surface of Eastern Elysium Planitia. Two geologic interfaces bounded by reflectors (L1R & L2R) are present below the surface. (B) Floods erupt from Cerberus Fossae and carve multiple channels between tear-drop shaped islands. (C) Further flooding concentrates erosion in a single large channel. (D) Eruption of Unit ACy lava flows buries portions of Unit ACo (including the eastern section of Cerberus Fossae) and fills the Marte Vallis channels. Black arrow indicates north.

Table S1.

Orbit Number	Reflectors Present	Orbit Number	Reflectors Present
340502000	*L1R and R3*	688603000	*L1R and L2R*
348402000	*L1R and L2R*	695202000	*L1R, L2R and R3*
369501000	*L1R and L2R*	703103000	*L1R and L2R*
376102000	*L1R, L2R and R3*	709703000	*L1R, L2R and R3*
382702000	*L1R, L2R and R3*	724203000	*L1R and L2R*
390601000	*L1R and L2R*	738701000	*L1R and L2R*
397201000	*L1R, L2R and R3*	752602000	*L1R, L2R and R3*
405101000	*L1R and L2R*	753202000	*L1R and L2R*
411701000	*L1R and L2R*	753902000	*L1R and L2R*
418301000	*L1R, L2R and R3*	760502000	*L1R and L2R*
439402000	*L1R, L2R and R3*	767703000	*L1R*
440702000	*L1R and L2R*	774302000	*L1R and L2R*
447302000	*L1R*	788802000	*L1R and L2R*
468401000	*L1R*	795401000	*L1R, L2R and R3*
483601000	*L1R*	803301000	*L1R and L2R*
504001000	*L1R and L2R*	804001000	*L1R and L2R*
518502000	*L1R and L2R*	809901000	*L1R, L2R and R3*
567301000	*L1R, L2R and R3*	838901000	*L1R and L2R*
568001000	*L1R and L2R*	839601000	*L1R and L2R*
575202000	*L1R and L2R*	845501000	*L1R, L2R and R3*
581801000	*L1R and L2R*	846802000	*L2R*
588402000	*L1R, L2R and R3*	867901000	*L1R and L2R*
617402000	*L1R*	882401000	*L1R and L2R*
624003000	*L1R, L2R and R3*	889001000	*L1R, L2R and R3*
653002000	*L1R*	896901000	*L1R and L2R*
659601000	*L1R, L2R and R3*	924601000	*L1R, L2R and R3*
667503000	*L1R and L2R*	932501000	*L1R and L2R*
674102000	*L1R, L2R and R3*	1809400000	*L1R, L2R and R3*
682102000	*L1R and L2R*	1922800000	*L1R, L2R and R3*

SHARAD tracks used in the study

References and Notes

1. D. H. Scott K. L. Tanaka, *Geological map of the western equatorial region of Mars. U.S. Geological survey Misc. Map I-1802-A* (1986).

2. K. L. Tanaka, The stratigraphy of Mars. *J. Geophys. Res.* **91**, (B13), E139 (1986). doi:10.1029/JB091iB13p0E139

3. S. Rotto, K. L. Tanaka, *Geologic/Geomorphic map of the Chryse Planitia region of Mars. U.S. Geological survey Misc. Inv. Map I-2441* (1995)

4. D. C. Berman, W. K. Hartmann, Recent fluvial, volcanic and tectonic activity on the Cerberus Plains of Mars. *Icarus* **159**, 1 (2002). doi:10.1006/icar.2002.6920

5. J. Vaucher *et al*., The volcanic history of central Elysium Planitia, implications for martian magmatism. *Icarus* **204**, 418 (2009). doi:10.1016/j.icarus.2009.06.032

6. D. M. Burr, J. A. Grier, A. S. McEwan, L. P. Keszthelyi, Reapeted aqueous flooding from the Cerberus Fossae: Evidence for very recent extant, deep groundwater on Mars. *Icarus* **159**, 53 (2002). doi:10.1006/icar.2002.6921

7. E. R. Fuller, J. W. Head, Amazonis Planitia: The role of geologically recent volcanism and sedimentation in the formation of the smoothest plains on Mars. *J. Geophys. Res.* **107**, (E10), 5081 (2002). doi:10.1029/2002JE001842

8. J. B. Murray *et al*.; HRSC Co-Investigator Team, Evidence from the Mars Express High Resolution Stereo Camera for a frozen sea close to Mars' equator. *Nature* **434**, 352 (2005). doi:10.1038/nature03379 Medline

9. J. B. Plescia, Cerberus Fossae, Elysium, Mars: A source for lava and water. *Icarus* **164**, 79 (2003).

10. R. Seu *et al*., SHARAD: The MRO 2005 shallow radar. *Planet. Space Sci.* **52**, 157 (2004). doi:10.1016/j.pss.2003.08.024

11. R. Seu *et al*., SHARAD sounding radar on the Mars Reconnaissance Orbiter. *J. Geophys. Res.* **112**, (E5), E05S05 (2007). doi:10.1029/2006JE002745

12. Materials and methods are available as supplementary materials on *Science* Online.

13. The time delay offset between a reflector and the surface echo within a radargram can be converted to depth. This depth estimation is inversely proportional to the square root of the assumed permittivity (ε') of the material above the reflector. Figures 2 to 4 assume an ε' of 8, consistent with dense, dry terrestrial lava flows. Applying a lower value for ε' would provide a greater depth estimate for each of the reflectors.

14. K. L. Tanaka, J. A. Skinner, T. M. Hare, *Geologic map of the northern plains of Mars, U. S. Geol. Surv. Sci. Invest. Map, 2888* (2005).

15. L. M. Carter *et al*., Dielectric properties of lava flows west of Ascraeus Mons, Mars. *Geophys. Res. Lett.* **36**, L23204 (2009). doi:10.1029/2009GL041234

16. C. S. Fulthorpe, J. A. Austin, Jr., Shallowly buried, enigmatic seismic stratigraphy on the New Jersey outer shelf: Evidence for latest Pleistocene catastrophic erosion? *Geology* **32**, 1013 (2004). doi:10.1130/G20822.1

17. M. Carr, Formation of martian flood features by release of water from confined aquifers. *J. Geophys. Res.* **84**, (B6), 2995 (1979). doi:10.1029/JB084iB06p02995

18. N. H. Warner, S. Gupta, J.-P. Muller, J.-R. Kim, S.-Y. Lin, A refined chronology of catastrophic outflow events in Ares Vallis, Mars. *Earth Planet. Sci. Lett.* **288**, 58 (2009). doi:10.1016/j.epsl.2009.09.008

19. W. L. Jaeger *et al*., Emplacement of the youngest flood lava on Mars: A short, turbulent story. *Icarus* **205**, 230 (2010). doi:10.1016/j.icarus.2009.09.011

20. D. W. Leverington, A volcanic origin for the outflow channels of Mars: Key evidence and major implications. *Geomorphology* **132**, 51 (2011). doi:10.1016/j.geomorph.2011.05.022

21. B. A. Campbell *et al*., SHARAD radar sounding of the Vastitas Borealis Formation in Amazonis Planitia. *J. Geophys. Res.* **113**, (E12), E12010 (2008). doi:10.1029/2008JE003177

22. F. T. Ulaby *et al*., Microwave dielectric spectrum of rocks, Rep. 23817-1-T, Univ. of Mich. Radiat. Lab., Ann Arbor (1988).

23. W. D. Carrier, G. R. Ohloeft, W. Mendell, Physical properties of the lunar surface, in G. H. Heiken, D. T. Vaniman, B. M. French Eds., *Lunar Sourcebook*, pp. 457–567, (Cambridge Univ. Press, New York, 1991).

24. V. R. Baker, D. Nummedal Eds., *The Channeled Scabland; a Guide to the Geomorphology of the Columbia Basin* (NASA, Washington, DC, 1978).

25. B. A. Campbell, N. E. Putzig, L. M. Carter, R. J. Phillips, Autofocus correction of phase distortion effects on SHARAD echoes. *IEEE Geosci. Remote Sens. Lett.* **8**, 939 (2011). doi:10.1109/LGRS.2011.2143692